

Co-combustion of *Spirulina (Arthrospira) platensis* and waste at a 30/70 mass ratio in a fluidized-bed combustor: residual ash characteristics, potential issues, and utilization

Sukarni Sukarni¹, Ivan Fahrizal¹, Ahmad Yusril Aminullah¹, Retno Wulandari¹, Prihanto Trihutomo¹, and Muhammad Shahbaz²

¹Center for Renewable Fuels Research (CRFR), Department of Mechanical and Industrial Engineering, Universitas Negeri Malang, Malang, Indonesia

²Net Zero Industry Innovation Centre, School of Computing, Engineering and Digital Technologies, Teesside University, Middlesbrough, United Kingdom

Abstract. Fossil-based solid fuel dependency is characterized by supply scarcity and environmental hazards, underscoring the need for cleaner, renewable energy sources. *Spirulina (Arthrospira) platensis* (SP) cyanobacterium is a promising source of energy due to its abundance and high calorific value. However, co-combustion is one of several methods to reduce environmental impact by utilizing unmanaged plastic or synthetic waste (SW) with high volatility and combining it with SP. Circulating fluidized bed combustor (CFBC) technology is one of the effective thermal methods to convert various types of feedstocks into a heat source. There is limited study about the co-combustion of microalgae and plastic waste in CFBC. This study aims to examine the ash characteristics of 30% SP and 70% SW. Ash characterization is important to mitigate ash buildup and evaluate its potential for valorization. Morphology analysis showed that combustion significantly alters the feedstock's physical structure, resulting in more porous, coarser ash. The main compositions of ash are O, Si, Cl, P, Na, and Fe. Fourier transform infrared (FTIR) spectroscopy revealed the loss of specific peaks in the 3700-2000 cm⁻¹ region after combustion, indicating the decomposition of proteins and lipids from SP, whereas the SW component showed significant polymer degradation.

1 Introduction

Indonesian energy sources consist of oil at 42%, then coal at 17%, electricity at 16%, natural gas at 10%, liquified petroleum gas at 7%, and biodiesel and biomass each at around 4% [1]. However, its limited availability and negative climate impact from greenhouse gas emissions underscore the need for renewable, clean energy sources. Biomass is considered a potential renewable energy source, especially microalgae. *Spirulina (Arthrospira) platensis* (SP) is a

¹ Corresponding author: sukarni.ft@um.ac.id

green-blue microalgae classified as a cyanobacterium, single-celled, and spiral-shaped. *Spirulina* can be cultivated under various conditions, reflecting its abundance, and has a high calorific value of 21 MJ/kg, higher than that of other feedstocks [2].

On the other hand, population growth also positively correlated with the growth of synthetic waste (SW). The production of global synthetic waste has recently reached 10,660 tonnes/day, while Indonesia is the second-largest contributor of marine synthetic waste debris. Uncontrollable waste treatment leads to garbage accumulation, as observed in Malang City. Incineration is considered a promising solution to reduce landfill overcapacity, driven by the availability of large quantities of synthetic waste.

The use of co-combustion feedstock consisting of biomass and waste is believed to have the potential to overcome energy and environmental problems. A controlled combustion process is required to achieve perfect combustion, which is typically achieved in incinerators such as circulating fluidized bed (CFB) units. Calado et al. [3] conduct co-combustion of waste tyre and miscanthus in a fluidized bed, resulting in a positive correlation between waste tyre loading and generated power, where maximum power is obtained at 156.91 kW for 60% waste tyre loading. CFB is a promising technology due to its flexibility, high combustion efficiency, and lower environmental impact than other incinerators. However, there is limited study about *Spirulina*-plastic co-combustion in a fluidized bed reactor, although the high calorific value of *Spirulina* offers better power generation and a smaller carbon footprint due to its superb CO₂ absorption ability. Research on the combustion characteristics of microalgae and synthetic waste in fluidized beds is still rare. Therefore, it is necessary to test *Spirulina platensis* microalgae and synthetic waste to determine the combustion characteristics. The purpose of this study is to determine the potential of *Spirulina platensis* microalgae and a synthetic waste mixture (30SP/70SW) as a solid fuel, as assessed by changes in morphology and functional groups.

2 Method

2.1 Material

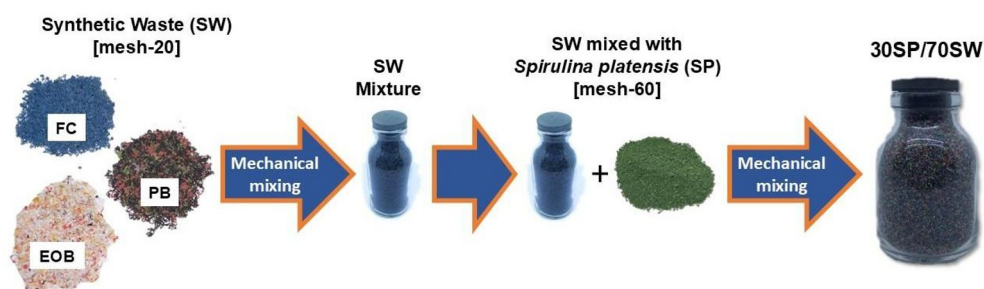


Fig. 1. 30SP/70SW combustion feedstock preparation

Spirulina platensis (SP) microalgae were obtained from the Balai Besar Pengembangan Budidaya Air Payau (BBPBAP) in Situbondo, Indonesia. SP powder is dried in the oven at 100°C for 24 hours. The dry material is then sifted through a 60-mesh (<0.25 mm) filter. Synthetic waste (SW) is collected from a landfill in Malang City, Indonesia. The composition of SW consists of engine oil bottles (EOB), plastic buckets (PB), and food containers (FC). This waste is cleaned with water and sun-dried for 2 days before being filtered to a 20-mesh (<0.84 mm) size. For the experiment, the two samples were mixed at a 30/70 (SP/SW) mass ratio using a mechanical mixer

at 1200 rpm for 15 minutes. The resulting mixture is weighed into 1 g portions for characterization and into 100 g portions for each combustion test.

2.2 Experimental setup

The blower supplies air to the reactor system at 7 m/s, as measured by an Anemometer. Silica sand with a particle size of less than 0.25 mm and a specific gravity of 1520 kg/m³ is fed into the reactor as a fluidization medium. The combustion chamber is initially heated with LPG until the third K-type thermocouple (T3) reaches a stable temperature of 750 °C. Then, the 30SP/70SW mixture is fed into the reactor using a feeder screw at a rate of 0.86 kg/min. The temperature of the screw feeder is controlled using a condenser to maintain the sample's temperature stability. After the stable combustion of the 30SP/70SW sample is achieved, the LPG flow is stopped, and the combustion process is allowed to stop independently. After the experiment, the CFBC unit is cooled until the second thermocouple (T2) shows a temperature below 100°C, and then the combustion residue is cleaned up. To improve data accuracy, all measurements are repeated three times.

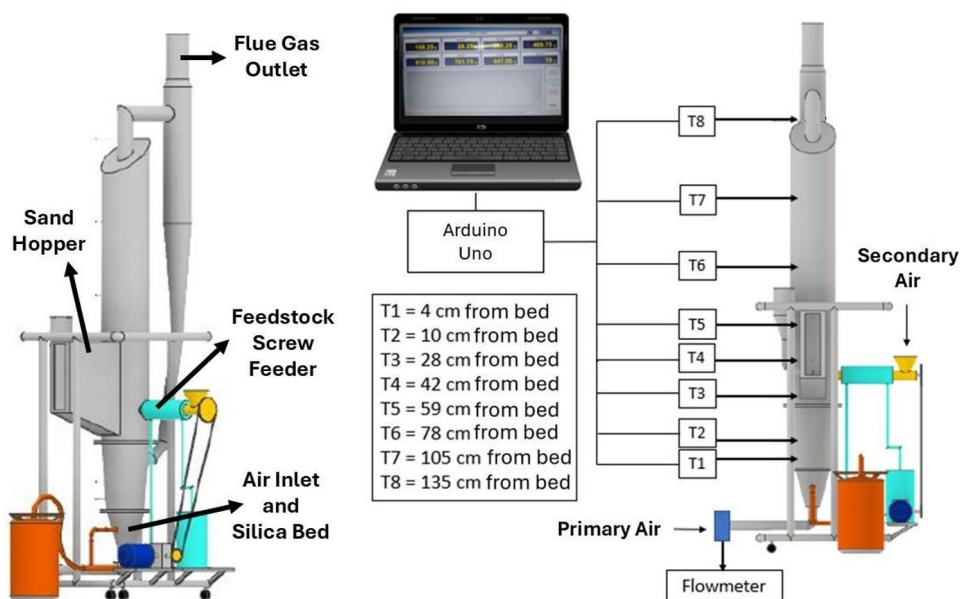


Fig. 2. Circulating fluidized-bed combustor

2.3 Characterization

SP and SW were analyzed for their raw materials and combustion byproducts. The surface morphological structures of the raw material and the pyrolysis byproduct were examined using SEM (Scanning Electron Microscopy) on an FEI Inspect S50. Functional group analysis was performed using Fourier Transform Infrared Spectroscopy (FTIR) on a Shimadzu IR Prestige-21 over a wavelength range of 4000–400 cm⁻¹.

3 Results and discussion

Figure 3 shows the morphological change of the mixture of 30SP/70SW before combustion or raw material and after combustion or ash from combustion. The 30SP/70SW raw material consists of non-porous particles with a size less than 500 μm ; particle size is directly related to combustion rate, as particles with a high surface area burn more quickly. Lu et al. [4] found that fuel particles with a large surface area have a higher reaction rate than those with a lower surface area. After combustion, the morphology of the 30SP/70SW ash particles differs from that of the raw material, with particle size decreasing and surface area increasing due to devolatilization and combustion. Okekunle et al. [5] found that devolatilization and combustion of fixed carbon during combustion led to a significant decrease in mass due to mass transfer from the solid to the gas phase.

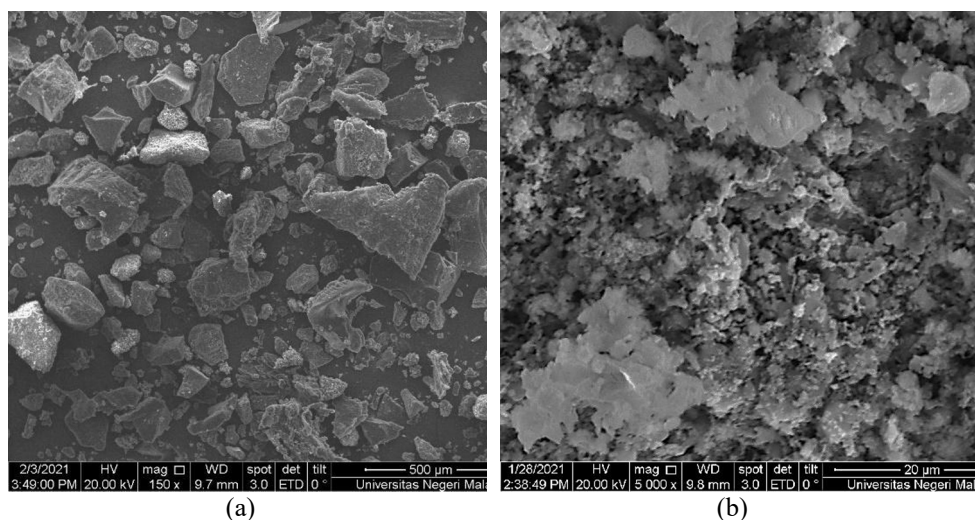


Fig. 3. 30SP/70SW (a) raw material (b) ash

Table 1 demonstrates that chemical analysis reveals a carbon content of 46.1% in 30SP/70SW, highlighting its utility as a combustion feedstock owing to its capacity as a heat source. After combustion, carbon is lost, most likely oxidized to form carbon dioxide gas. Several elements have just emerged in ash, including silicon, magnesium, phosphorus, titanium, and iron. These elements can be attributed to macroalgae and microalgae nutrients and additives in SW [6,7]. The incombustible nature of these elements causes the formation of ash. The phosphorus and potassium content indicate the potential of 30SP/70SW ash as a fertilizer.

Table 1. Elemental composition comparison of 30SP/70SW raw material and its ash

| Sample | Chemical content (wt.%) | | | | | | | | | | | |
|--------|-------------------------|-------|------|------|-------|------|------|------|------|------|------|------|
| | C | O | Na | Al | Si | Cl | Ca | K | Mg | P | Ti | Fe |
| Raw | 46.1 | 38.32 | 4.19 | 0.85 | - | 5.6 | 3.72 | 2.6 | - | - | - | - |
| Ash | - | 39.68 | 7.46 | 1.14 | 16.62 | 8.08 | 4.94 | 5.53 | 2.61 | 6.74 | 0.71 | 6.49 |

Analysis of the functional group of raw material and ash of 30SP/70SW showed a significant difference (Figure 4) where the functional group associated with SP microalgae such as C-H and

C-O from carbohydrates ($1800-1200\text{ cm}^{-1}$) and N-H from proteins in the range of $900-700\text{ cm}^{-1}$, while the SW group consisting of aliphatic group (CH_2) in the wavenumber range of $3100-2800\text{ cm}^{-1}$ (Table 2) was not detected in the 30SP/70SW ash spectrum. Volatile substances and fixed carbon will be converted into gaseous phases due to combustion, which is confirmed by EDX results (Table 1), where carbon elements are not detected due to the loss of carbon-containing functional groups such as C-H, C-O, C=O, and CH_2 .

Table 2. Functional group band assignment of 30SP/70SW raw material

| No. | Peak (cm^{-1}) | Range (cm^{-1}) | Band Assignment | Reference |
|-----|---------------------------|----------------------------|-----------------------------------------------------------------------------------------------------------------------------------------------------------------------------------------------------------------------------------------------------------------------------------------------------------------------------------------------------|-----------|
| 1 | 700.16 | 707.8-675.0 | <ul style="list-style-type: none"> ● C-H bending; aromatic groups ● N-H wag; amide II | [8] |
| 2 | 840.96 | 862.1-823.6 | <ul style="list-style-type: none"> ● C-H bending; aromatic groups ● C₄-O-S (sulfate) ● NH₂ out of plane; amide I | [8] |
| 3 | 898.83 | 906.5-891.1 | <ul style="list-style-type: none"> ● C-H bending; aromatic groups | [8] |
| 4 | 939.33 | 947.0-923.9 | <ul style="list-style-type: none"> ● $\nu(\text{C}-\text{O}-\text{C})$ of polysaccharides ● $-\text{CH}-\text{CH}_2$ (bond =CH) vinyl | [9] |
| 5 | 972.12 | 983.6-950.9 | <ul style="list-style-type: none"> ● $\nu\text{C}-\text{O}/\nu\text{Si}-\text{O}$; carbohydrates/siloxanes ● $\nu(\text{C}-\text{O}-\text{C})$ of polysaccharides | [8] |
| 6 | 1103.28 | 1110.9-1066.6 | <ul style="list-style-type: none"> ● $\nu\text{C}-\text{O}/\nu\text{Si}-\text{O}$; carbohydrates/siloxanes ● Symmetric C-H stretching vibration. ● C-O stretching saturated ethers | [10] |
| 7 | 1166.93 | 1182.3-1151.5 | <ul style="list-style-type: none"> ● Carbohydrate $\nu(\text{C}-\text{O}-\text{C})$ of polysaccharides ● $\nu\text{C}-\text{O}/\nu\text{Si}-\text{O}$; carbohydrates/siloxanes | [11] |
| 8 | 1255.66 | 1263.3-1228.6 | <ul style="list-style-type: none"> ● C-O asymmetric C-O-C stretching presence of esters. ● C-O stretching; unsaturated ethers | [8] |
| 9 | 1377.17 | 1382.9-1363.6 | <ul style="list-style-type: none"> ● Protein $\delta\text{s}(\text{CH}_2)$ and $\delta\text{s}(\text{CH}_3)$ bending of methyl carboxylic acid vs(C-O) of COO- groups of carboxylates ● Lipid $\delta\text{s}(\text{N}(\text{CH}_3)_3)$ bending of methyl ● O-H & C-H bending | [11] |
| 10 | 1454.33 | 1458.1-1446.6 | <ul style="list-style-type: none"> ● Protein $\delta\text{as}(\text{CH}_2)$ and $\delta\text{as}(\text{CH}_3)$ bending of methyl, ● Lipid $\delta\text{as}(\text{CH}_2)$ bending of methyl ● $\nu\text{C}-\text{O}$ carboxylic group ● C-H bending | [11] |
| 11 | 2183.42 | 2179.5-2189.2 | <ul style="list-style-type: none"> ● stretching vibrations of carboxyl and carbonyl C=O | [12] |
| 12 | 2239.36 | 2223.9-2245.1 | <ul style="list-style-type: none"> ● $-\text{C}\equiv\text{N}$ Nitriles | [13] |
| 13 | 2661.77 | 2648.2-2669.4 | <ul style="list-style-type: none"> ● (O=)PO-H phosphonic acid ● -CHO aldehydes | [13] |
| 14 | 2920.23 | 2937.5-2881.6 | <ul style="list-style-type: none"> ● Lipid - carbohydrate CH_2 stretching ● CH and CH_2 aliphatic group | [11] |
| 15 | 3184.48 | 3188.3-3180.6 | <ul style="list-style-type: none"> ● Water $\nu(\text{O}-\text{H})$ stretching protein $\nu(\text{N}-\text{H})$ stretching (amide A) | [11] |

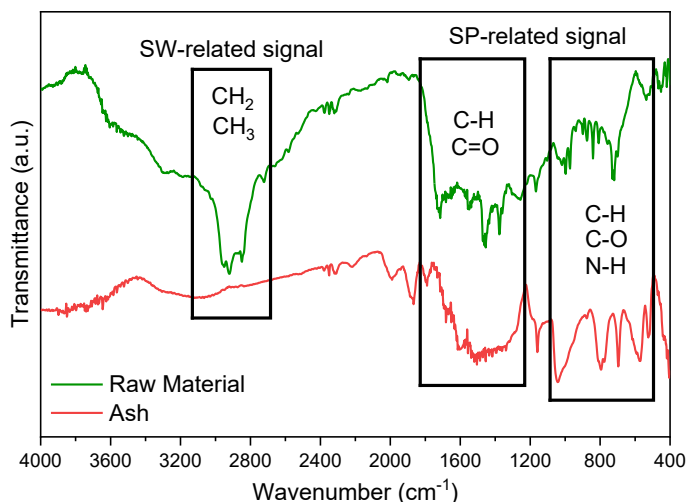


Fig. 4. FTIR Spectra of 30SP/70SW

Table 3 shows the identity of the peak of the ash spectrum, where the functional group in 30SP/70SW ash is dominated by incombustible elements such as Ca, Fe, Si, Mg, Mn, and P [14]. Band assignment analysis was confirmed by EDX results, which showed Si, Ca, and P as the dominant elements at 16.61, 8.08, and 6.74, respectively. These elements can cause fouling and clogging in the reactor, reducing heat transfer and power plant efficiency and requiring regular maintenance. Inorganic elements in the SP and SW mixture can be mitigated through various approaches, such as acid washing and an additional flue gas scrubber, to minimize downtime. However, SP30/SW70 ash contains a considerable amount of silica, which can be used to enhance adsorption selectivity for water treatment purposes.

Table 3. Functional group band assignment of 30SP/70SW ash

| No. | Peak (cm ⁻¹) | Range (cm ⁻¹) | Band Assignment | Reference |
|-----|--------------------------|---------------------------|----------------------------------------------------------------------------------------------------------|-----------|
| 1 | 524.64 | 497.6-528.4 | • M–O vibrations, particularly, Ca–O, Fe–O, Mn–O, and Mg–O vibrations | [14] |
| 2 | 1041.56 | 1001.0-1056.9 | • Si–O–Si | [14] |
| 3 | 1286.52 | 1224.7-1290.3 | • Si–O • Organic Phosphate (P=O) | [14] |
| 4 | 1317.38 | 1311.5-1321.2 | • Asymmetric stretching -SO ₂ ; Sulfones • P–O Phosphorus • Organic Phosphate (P=O) | [14] |
| 5 | 1338.6 | 1334.7-1342.4 | • Asymmetric stretching -SO ₂ ; Sulfonamides • P–O Phosphorus • Organic Phosphate (P=O) | [14] |
| 6 | 1361.74 | 1355.9-1363.6 | • P–O Phosphorus | [14] |
| 7 | 1867.09 | 1843.9-1870.9 | • Si–OH groups stretching | [15] |
| 8 | 3280.92 | 3277.0-3282.8 | • Si–OH groups stretching | [15] |

4 Conclusion

30SP/70SW is characterized and combusted to assess its potential as a solid fuel, with the raw material consisting of non-porous particles below 500 μm that undergo size reduction and increased surface area post-combustion due to devolatilization. High initial carbon content (46.1%) positively correlated with its energy content. Complete combustion is achieved with 30SP/70SW, as evidenced by efficient carbon oxidation, yielding carbon-free ash. FTIR analysis of ash also shows the absence of several functional groups, such as C-H, C-O, and CH_2 , which are associated with proteins, carbohydrates, and polymers in the 30SP/70SW raw material, indicating thermal degradation of those compounds and the release of heat energy. Given the absence of carbon in the ash, co-combustion of 30SP/70SW has high efficiency and represents a path to future scalability for substituting for solid fossil-based fuels. Inorganic elements such as Si, Ca, P, and Mg originating from microalgae nutrients and synthetic waste additives form ash due to their incombustible nature. While these inorganics may contribute to operational challenges like fouling and reactor clogging, the appreciable levels of phosphorus and potassium suggest potential for ash valorization as fertilizer. Additionally, the high silica content offers opportunities to repurpose the ash for adsorption applications, such as water treatment. Thus, while combustion of 30SP/70SW is effective for energy recovery, attention to ash management is essential to mitigate fouling risks and leverage its nutrient and material recovery potential.

Acknowledgement. This research was fully funded by Universitas Negeri Malang through the Kompetitif Topik KBK scheme, under contract number 24.2.209/UN32.14.1/LT/2025.

References

1. Badan Pengkajian dan Penerapan Teknologi (BPPT), *OUTLOOK ENERGI INDONESIA 2021 Perspektif Teknologi Energi Indonesia: Tenaga Surya untuk Penyediaan Energi Charging Station*, (2021)
2. M.S. Ghayal, M.T. Pandya, *Microalgae Biomass: A Renewable Source of Energy*, *Energy Procedia*. **32**, 242–250 (2013). doi:10.1016/J.EGYPRO.2013.05.031.
3. L. Carmo-Calado, M.J. Hermoso-Orzáez, R. Mota-Panizio, B. Guilherme-Garcia, P. Brito, *Co-Combustion of Waste Tires and Plastic-Rubber Wastes with Biomass Technical and Environmental Analysis*, *Sustainability* 2020, Vol. **12**, Page 1036. 1036 (2020). doi:10.3390/SU12031036.
4. H. Lu, E. Ip, J. Scott, P. Foster, M. Vickers, L.L. Baxter, *Effects of particle shape and size on devolatilization of biomass particle*, *Fuel*. **89**, 1156–1168 (2010). doi:10.1016/j.fuel.2008.10.023.
5. P.O. Okekunle, H. Watanabe, T. Pattanotai, K. Okazaki, *Effect of biomass size and aspect ratio on intra-particle tar decomposition during wood cylinder pyrolysis*, *Journal of Thermal Science and Technology*. **7**, 1–15 (2012). doi:10.1299/jtst.7.1.
6. Sukarni, Sumarli, P. Puspitasari, H. Suryanto, R.F. Wati, *Physicochemical characteristics of various inorganic combustible solid waste (ICSW) mixed as sustainable solid fuel*, in: *AIP Conf. Proc.*, 2017: p. 020066. doi:10.1063/1.5003549.
7. S. Sukarni, U. Yanuhar, I.N.G. Wardana, S. Sudjito, N. Hamidi, W. Wijayanti, Y. Wibisono, S. Sumarli, I.M. Nauri, H. Suryanto, *Combustion of Microalgae Nannochloropsis oculata Biomass: Cellular Macromolecular and Mineralogical Content Changes During Thermal Decomposition*, *Songklanakarin Journal of Science and Technology*. **40**, 1456–1463 (2018). doi:10.14456/sjst-psu.2018.178.

8. A. Lecellier, J. Mounier, V. Gaydou, L. Castrec, G. Barbier, W. Ablain, M. Manfait, D. Toubas, G.D. Sockalingum, Differentiation and identification of filamentous fungi by high-throughput FTIR spectroscopic analysis of mycelia, *Int. J. Food Microbiol.* **168–169**, 32–41 (2014). doi:10.1016/J.IJFOODMICRO.2013.10.011.
9. P. Heraud, B.R. Wood, M.J. Tobin, J. Beardall, D. McNaughton, Mapping of nutrient-induced biochemical changes in living algal cells using synchrotron infrared microspectroscopy, *FEMS Microbiol. Lett.* **249**, 219–225 (2005). doi:10.1016/J.FEMSLE.2005.06.021.
10. P. FU, S. HU, J. XIANG, L. SUN, T. YANG, A. ZHANG, J. ZHANG, Mechanism Study of Rice Straw Pyrolysis by Fourier Transform Infrared Technique, *Chin. J. Chem. Eng.* **17**, 522–529 (2009). doi:10.1016/S1004-9541(08)60240-2.
11. Dilek (Yalcin) Duygu, Fourier transform infrared (FTIR) spectroscopy for identification of *Chlorella vulgaris* Beijerinck 1890 and *Scenedesmus obliquus* (Turpin) Kützing 1833, *Afr. J. Biotechnol.* **11**, 3817–3824 (2012). doi:10.5897/ajb11.1863.
12. J. Eshun, L. Wang, E. Ansah, A. Shahbazi, K. Schimmel, V. Kabadi, S. Aravamudhan, Characterization of the physicochemical and structural evolution of biomass particles during combined pyrolysis and CO₂ gasification, *Journal of the Energy Institute.* 1–12 (2017). doi:10.1016/j.joei.2017.11.003.
13. K.J. Gaffney, P.H. Davis, I.R. Piletic, N.E. Levinger, M.D. Fayer, Hydrogen bond dissociation and reformation in methanol oligomers following hydroxyl stretch relaxation, *Journal of Physical Chemistry A.* **106**, 12012–12023 (2002). doi:10.1021/jp021696g.
14. R. Abraham, J. George, J. Thomas, K.K.M. Yusuff, Physicochemical characterization and possible applications of the waste biomass ash from oleoresin industries of India, *Fuel.* **109**, 366–372 (2013). doi:10.1016/J.FUEL.2013.02.067.
15. S. Munshi, R.P. Sharma, Investigation on the pozzolanic properties of rice straw ash prepared at different temperatures, *Materials Express.* **8**, 157–164 (2018). doi:10.1166/MEX.2018.1416.